

# Testing and Evaluation of Polyurethane-Based GFRP Sandwich Bridge Deck Panels with Polyurethane Foam Core

Hesham Tuwair<sup>1</sup>; Jeffery Volz<sup>2</sup>; Mohamed A. ElGawady, M.ASCE<sup>3</sup>; Mohaned Mohamed<sup>4</sup>; K. Chandrashekhara<sup>5</sup>; and Victor Birman<sup>6</sup>

**Abstract:** This paper presents the evaluation of an innovative low-cost small-scale prototype deck panel under monotonic and fatigue bending. This new system introduces a trapezoidal-shaped polyurethane foam core with a thermoset polyurethane resin that has a longer pot life to facilitate the infusion process. The proposed panel exhibited a higher structural performance in terms of flexural stiffness, strength, and shear stiffness. The panels consist of two glass fiber-reinforced polymer (GFRP) facings with webs of bidirectional E-glass-woven fabric that are separated by a trapezoidal-shaped low-density polyurethane foam. The GFRP panels were manufactured using a one-step vacuum-assisted resin transfer molding process. The specimens studied were constructed in the Composite Manufacturing Laboratory in the Mechanical and Aerospace Engineering Department at Missouri University of Science and Technology. Small-scale prototype deck panels were tested both statically and dynamically in four-point bending to investigate their flexural behavior. The ultimate bearing capacity of the proposed sandwich panels was determined from compression crushing tests. In addition, the load-deflection behavior of the proposed panel was investigated under three loading conditions: compression, static flexure, and dynamic flexure. The initial failure mode for all panels was localized outward-compression skin wrinkling of the top facing. The ultimate failure was caused by local crushing of the top facing under the loading point due to excessive compressive stresses. First-order shear deformation theory was used to predict the panel deformation in the service limit state. In general, the analytical results were found to be in good agreement with the experimental findings. DOI: 10.1061/(ASCE)BE.1943-5592.0000773. © 2015 American Society of Civil Engineers.

**Author keywords:** FRP bridge deck; Sandwich panels; GFRP; Polyurethane foam.

## Introduction

According to a study conducted by the Federal Highway Administration (FHWA), 152,000 out of 607,000 bridges (25%) in the United States are in need of either repair or replacement owing to corrosion of concrete steel reinforcement (Kirk and Mallett 2013). Replacement of deficient bridges at low costs represents an important challenge. Fiber-reinforced polymer (FRP) has shown great promise as a potential construction material for construction of bridges (e.g., Abdelkarim and ElGawady 2014; Dawood and ElGawady 2013; ElGawady and Sha'lan 2011; ElGawady and

Dawood 2012; ElGawady et al. 2010). Using FRP eliminates corrosion issues and meets the goal of a 100-year life span. Although FRP bridges are cost effective over their life cycle, high initial costs hamper their use. Currently, more than 50 FRP bridges are in service in the United States. For example, the No-Name Creek Bridge, built in Kansas in 1996, was the first FRP honeycomb sandwich bridge (Ji et al. 2010). However, honeycomb sandwich construction requires a labor-intensive manufacturing process that increases the cost of FRP panels and lengthens the lead time. As a result, honeycomb systems, which have primarily been used in the aerospace industry, represent a rather questionable value in bridge applications.

Fiber-reinforced polymer sandwich structures offer a number of advantages including high strength, high flexural stiffness, reduced weight, environmental resistance, rapid construction, and ease of installation compared with conventional bridge materials such as steel or concrete. Fiber-reinforced polymer bridge decks weigh approximately one-fifth of an equivalent reinforced concrete deck (Murton 1999). However, low strength of the core is among the challenges faced by sandwich structures, including those used in bridge decks. Delamination of layers of the facings and debonding of the facings from the core present additional challenges. For example, the study conducted by Camata and Shing (2010) on structural and fatigue response of sandwich bridge decks revealed that delamination failure between the facings and the honeycomb core was the principal mode of failure. A number of studies have been conducted to develop better and more reliable FRP bridge decks. For example, Hassan et al. (2003) proposed an alternative system for FRP bridge decks using three-dimensional fibers (also known as through-thickness fiber), which were manufactured using either weaving or injection technology. These fibers were used to connect the top and bottom glass fiber-reinforced polymer (GFRP)

<sup>1</sup>Graduate Research Assistant, Dept. of Civil, Architectural, and Environmental Engineering, Missouri Univ. of Science and Technology, Rolla, MO 65401. E-mail: hrthw2@mst.edu

<sup>2</sup>Associate Professor, School of Civil Engineering and Environmental Science, Univ. of Oklahoma, Norman, OK 73019. E-mail: volz@ou.edu

<sup>3</sup>Associate Professor, Dept. of Civil, Architectural, and Environmental Engineering, Missouri Univ. of Science and Technology, Rolla, MO 65401 (corresponding author). E-mail: elgawadym@mst.edu

<sup>4</sup>Graduate Research Assistant, Dept. of Mechanical and Aerospace Engineering, Missouri Univ. of Science and Technology, Rolla, MO 65401. E-mail: mmm7vc@mst.edu

<sup>5</sup>Curators' Professor, Dept. of Mechanical and Aerospace Engineering, Missouri Univ. of Science and Technology, Rolla, MO 65401. E-mail: chandra@mst.edu

<sup>6</sup>Professor, Engineering Education Center, Missouri Univ. of Science and Technology, St. Louis, MO 63131. E-mail: vbirman@mst.edu

Note. This manuscript was submitted on August 7, 2014; approved on December 29, 2014; published online on June 6, 2015. Discussion period open until November 6, 2015; separate discussions must be submitted for individual papers. This paper is part of the *Journal of Bridge Engineering*, © ASCE, ISSN 1084-0702/04015033(13)/\$25.00.

facings and thus overcome delamination in the facings and debonding between the facings and core. The proposed design also enhanced strength and stiffness over traditional sandwich composites. A somewhat similar approach was considered by Potluri et al. (2003), who found that the mechanical, structural, and fatigue properties of FRP panels improved significantly when stitches were added to connect the top and bottom skins. Rocca and Nanni (2005) investigated the flexural and fatigue behavior of GFRP sandwich panels that contained a fiber-reinforced foam core and found that the residual compressive strength was not significantly reduced after 2 million fatigue cycles. They also observed that the deflection associated with the shear contribution (in the total deflection) can be ignored because of the shear strength provided by the core. Zi et al. (2008) proposed a new type of GFRP bridge deck consisting of GFRP with rectangular holes filled with polyurethane foam. Their study found that, when the rectangular holes were filled with polyurethane foam, the structural response and strength in the transverse direction were significantly improved. However, the elastic modulus (i.e., stiffness) did not increase.

Recently, a comprehensive research program was conducted at Missouri University of Science and Technology to evaluate the static and fatigue behavior of an innovative sandwich panel system consisting of GFRP facings separated by a trapezoidal-shaped polyurethane foam core (Fig. 1) where the top and bottom facings were connected with corrugated shear layers. The present study investigated the monotonic and fatigue flexural strength of the proposed prototype panels. Material characterization through tensile and compressive coupon tests was also completed. The ultimate bearing capacity, local buckling, and crushing load were estimated through flatwise compressive tests of small-scale prototype panels. Finally, the analytical beam theory was used to predict the deflection of the tested specimens. The overall flexural strength and stiffness were determined by testing two GFRP sandwich panels in a four-bending load test, which was subsequently



Fig. 1. Sandwich panel system used in experiments

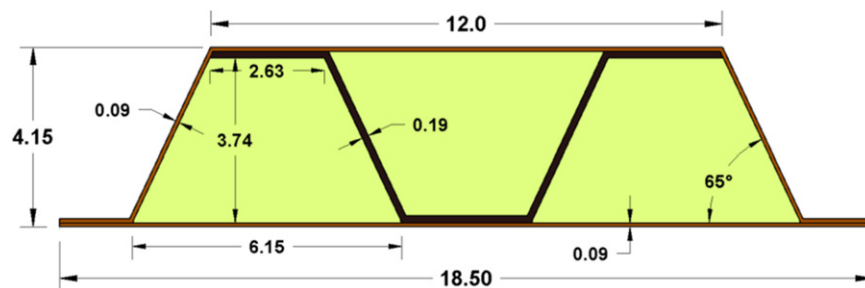


Fig. 2. Schematic of cross section (all dimensions in inches, 1 in. = 25.4 mm)

compared with an analytical prediction using the first-order shear deformation theory (FSDT) within the elastic region.

## Panel Description and Manufacturing

The cross-sectional dimensions of the panels considered in the study are shown in Fig. 2. The top and bottom facings of the panel are constructed with three layers of plain-weave woven E-glass fabric (WR18/20) laid up in  $0/90^\circ$  fiber orientation. The fibers were purchased from Owens Corning (Toledo, Ohio) and infused with a new type of longer pot life, i.e., a thermoset polyurethane resin that was developed by Bayer Material Science (Pittsburgh). The webs of the panels consist of corrugated shear layers (E-BXM1715), purchased from Vectorply (Phenix City, Alabama) and formed by three layers of  $\pm 45^\circ$  double bias, and the foam was matted with a combination of two plies and knitted E-glass laid up in  $\pm 45^\circ$  to produce better bond. The mass density of closed-cell polyurethane foam used in the core was  $32 \text{ kg/m}^3$  ( $2 \text{ lb/ft}^3$ ), purchased from Structural Composites (Melbourne, Florida). The sandwich panels were fabricated using a one-step vacuum-assisted resin transfer molding (VARTM) process, which has lower production costs compared with other manufacturing methods. The polyurethane foam was selected to be compatible with the polyurethane resin systems as well as to further reduce the manufacturing costs and panel weight. The new thermoset polyurethane resin that was used in this study has improved properties compared with commonly used polyester and vinyl ester resin systems (Connolly et al. 2006).

## Material Characterization

### Glass Fiber-Reinforced Polymer Facing and Web Characterization

To specify mechanical properties of the sandwich panels, three GFRP coupons were cut from the facings, and another three were cut from the web. All coupons were tested under tension, as shown in Fig. 3, according to the ASTM D3039/D3039M-08 standard (ASTM 2008a). All specimens were 254 mm (10 in.) long, 25.40 mm (1 in.) wide, and had the thickness of the corresponding element of the sandwich panel. End tabs were 63.50 mm (2.5 in.) long. The tension test was conducted with an MTS-880 universal testing machine (MTS Headquarters, Eden Prairie, Minnesota) at a loading rate of 1.27 mm/min (0.05 in./min), as recommended by the ASTM standard. Both longitudinal and transverse strains were recorded at the middle of the coupons using  $350 \Omega$  strain gauges produced by Micro Measurements Group (Wendell, North Carolina). Additionally, three facings and three web coupons were tested in compression according to the ASTM D3410/D3410M-03

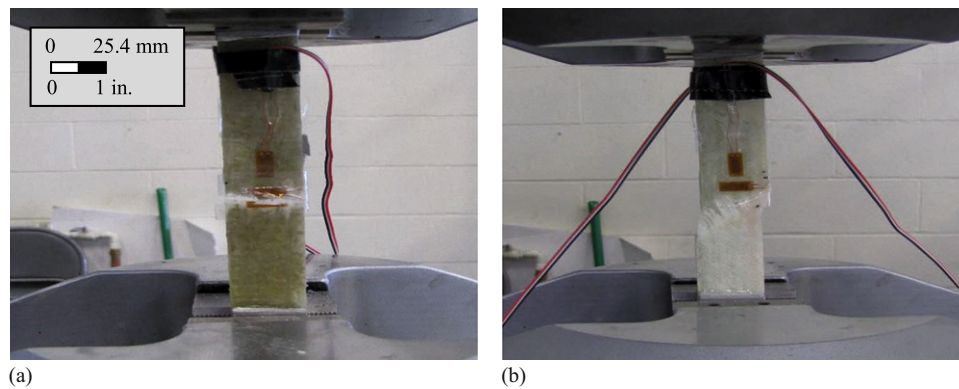


**Fig. 3.** Failure of (a) GFRP facings; (b) web layers

**Table 1.** Material Properties from Tensile Coupon Tests

Coupon type	Width, mm (in.)	Thickness, mm (in.)	Tensile modulus, MPa (ksi)			Ultimate strength, MPa (ksi)			Ultimate strain, in./in., mm/mm		
			Mean	SD <sup>a</sup>	COV <sup>b</sup>	Mean	SD	COV	Mean	SD	COV
Facing	25.40 (1)	2.89 (0.09)	13,977 (2,027.2)	131.7 (19.1)	0.94	264.8 (38.4)	15.9 (2.3)	6.1	0.019	0.001	5.88
Web core	25.40 (1)	4.83 (0.19)	11,803.1 (1,711.9)	938.4 (136.1)	7.95	176.5 (25.6)	9.7 (1.4)	5.5	0.03	0.004	14.06

<sup>a</sup>Standard deviation.

<sup>b</sup>Coefficient of variation (%).

**Table 2.** Material Properties from Compressive Coupon Tests

Coupon type	Width, mm (in.)	Thickness, mm (in.)	Compressive modulus, MPa (ksi)			Ultimate strength, MPa (ksi)			Ultimate strain, in./in., mm/mm		
			Mean	SD <sup>a</sup>	COV <sup>b</sup>	Mean	SD	COV	Mean	SD	COV
Facing	25.40 (1)	2.89 (0.09)	13,233 (1,919.3)	1711.3 (248.2)	12.9	102.7 (14.9)	16.27 (2.36)	15.8	0.011	0.004	34.66
Web core	25.40 (1)	4.83 (0.19)	7,260.2 (1,053)	1,088.7 (157.9)	15	128.7 (18.6)	9.5 (1.38)	7.41	0.024	0.005	22.90

<sup>a</sup>Standard deviation.

<sup>b</sup>Coefficient of variation (%).

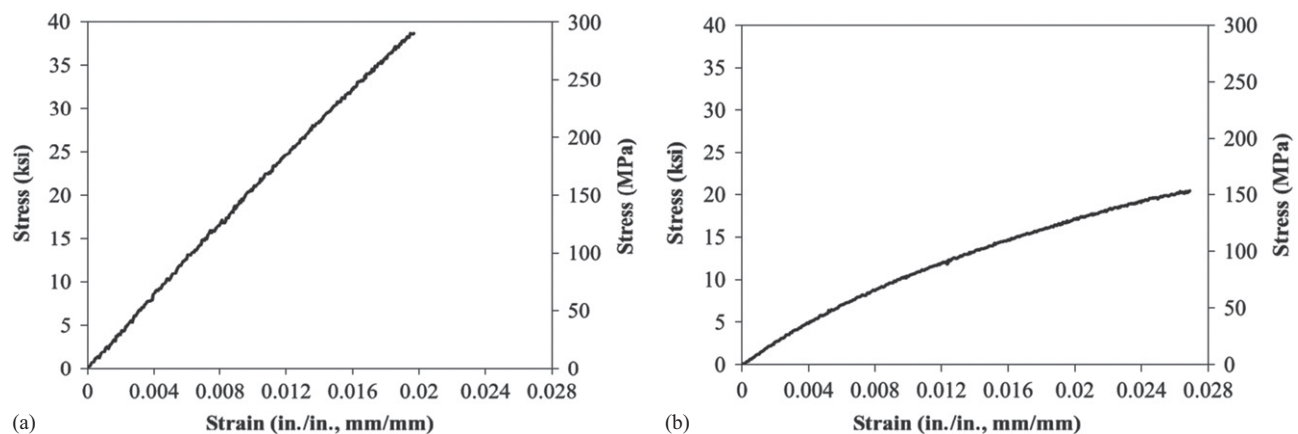


**Fig. 4.** Average tensile stress–strain curves for (a) GFRP facings; (b) web layers

standard (ASTM 2008b). Each coupon was 147.32 mm (5.8 in.) long and 25.40 mm (1 in.) wide with a gauge length of 20.32 mm (0.8 in.). The crosshead speed of the compression test was set at 0.127 mm/min (0.005 in./min) per the recommendation of the ASTM D3410/D3410M-03 standard (ASTM 2008b). Two strain gauges were attached to the coupons to measure the longitudinal and transverse strains within the gauge length.

Tables 1 and 2 summarize the coupon test results. The longitudinal tensile average stress–strain curves of the facings and web

coupons are shown in Figs. 4(a and b), respectively. The failure mode for all facing coupons was a sudden kink rupture, as shown in Fig. 3(a), whereas the failure mode for all web core coupons was shear rupture away from the gripping region, as observed in Fig. 3(b). The facings exhibited a linear elastic response up to an ultimate stress of approximately 264.7 MPa (38.4 ksi) corresponding to an ultimate strain of 0.019 mm/mm (in./in.). The web coupons displayed a slight softening nonlinearity that may be due to the orientation angle of the fiber (i.e., 45°/–45° double

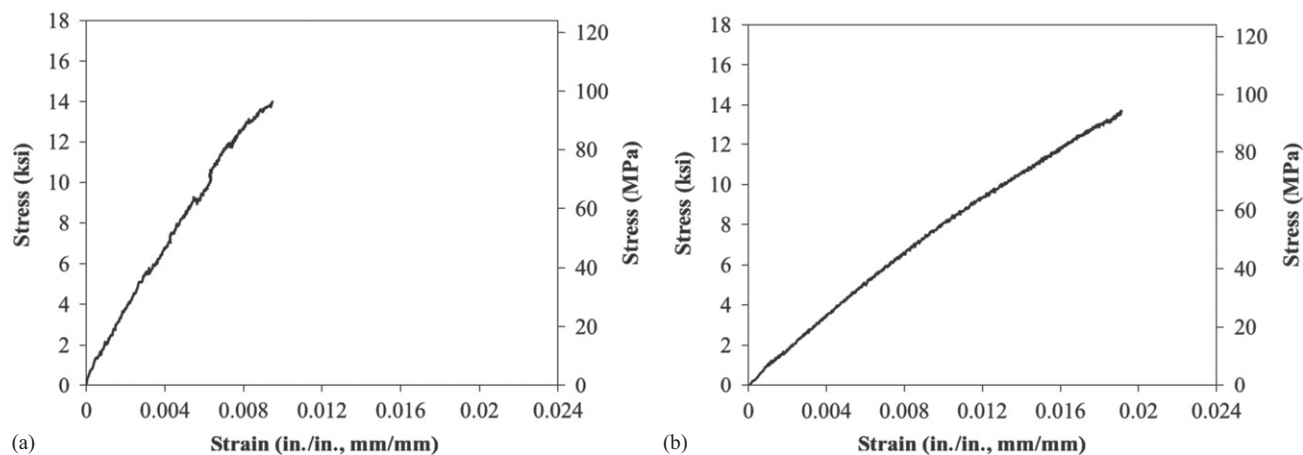


**Fig. 5.** Average compressive stress–strain curves for (a) GFRP facings; (b) web layers

bias) because the fibers will attempt to align with the direction of the applied load. The ultimate strain was approximately 0.027 mm/mm (in./in.) at an ultimate stress of 175.8 MPa (25.5 ksi). These properties are also valid in the transverse direction for both the facings and web core because of the symmetric architecture of the reinforcing fibers.

The axial compressive average stress–strain curves for the facings and web core are shown in Figs. 5(a and b), respectively. All compressed coupons failed when the fibers buckled and kinked. The ultimate compressive strengths of the facings and web were approximately 39 and 73% of their ultimate tensile strength, respectively.

### Foam Core Characterization

Three cubes of polyurethane foam were tested according to the ASTM C365/C365-11a standard (ASTM 2011a) to determine their compressive properties. Both the coupon dimensions and the mechanical properties of the tested specimens are listed in Table 3. Because the foam is very sensitive to small displacements, the testing was conducted with an Instron 4469 testing machine (Instron Worldwide Headquarters, Norwood, Massachusetts), which can provide very accurate measurements. All specimens were loaded using displacement control at a loading rate of 3.81 mm/min (0.15 in./min). This displacement rate was chosen to produce failure within 3–6 minutes per the recommendations of the ASTM C365/C365-11a standard (ASTM 2011a). The compressive stress–strain curves displayed in Fig. 6(a) demonstrate that the foam behaved linearly up to an average stress of 0.056 MPa (8.1 psi). The onset of nonlinear behavior occurred when the internal walls and struts of the foam architecture started collapsing. No visible signs of failure were observed until densification of the foam occurred [see Fig. 6(b)]. However, a visual inspection of the collapsed foam showed high residual displacements after unloading.

### Small-Scale Panel Tests

#### Crushing Test Setup

The objective of this test was to determine the ultimate bearing capacity of the sandwich panel, the local buckling load, and the failure modes. The tests were conducted on an MTS-880 testing machine with a load rate of 2.54 mm/min (0.1 in./min) (Fig. 7). Two specimens having the same cross section shown in Fig. 2, with

**Table 3.** Material Properties from Compressive Tests

Property	Measurement
Width, mm (in.)	64.26 (2.53)
Length, mm (in.)	65.79 (2.59)
Thick., mm (in.)	69.34 (2.73)
Elastic modulus, MPa (psi)	
Mean	2.1 (301.8)
SD	0.15 (21.5)
COV	7.1
Compressive strength, MPa (psi)	
Mean	0.056 (8.1)
SD	0.0034 (0.5)
COV	6.9
Compressive strain, in./in. mm/mm	
Mean	0.025
SD	0.005
COV	21.45

a length of 317.50 mm (12.5 in.), were cut from the panels and tested in flatwise compression up to failure. High-resistance rubber pads with a shore A hardness of 60 and thick steel plates were placed between the specimen and the contact surfaces to uniformly distribute the load. The applied load and the displacement of the crosshead of the testing machine were recorded during testing.

#### Flexural Test Setup

The objective of the flexural testing was to record the flexural behavior of the sandwich panel. The sandwich panels were tested under four-point loading according to the ASTM C393-11e1 standard (ASTM 2011b). Two sandwich specimens, subsequently referred to as 1-CP and 2-CP, were tested in one-way bending under two equal point loads, as shown in Figs. 8 and 9. The span length for the panel measured 1,092.20 mm (43 in.) with the point loads applied at a distance of 393.70 mm (15.5 in.) from each support. Each specimen was loaded up to failure, at a loading rate of 1.27 mm/min (0.05 in./min), in an MTS-880 universal testing machine.

A steel beam fixture was constructed and attached to the testing machine, as shown in Fig. 8. The beam base consisted of two hollow structural section (HSS) hollow steel sections welded laterally to provide the required width and capacity. Two cylindrical steel supports with diameters of 25.40 mm (1.0 in.) were welded to

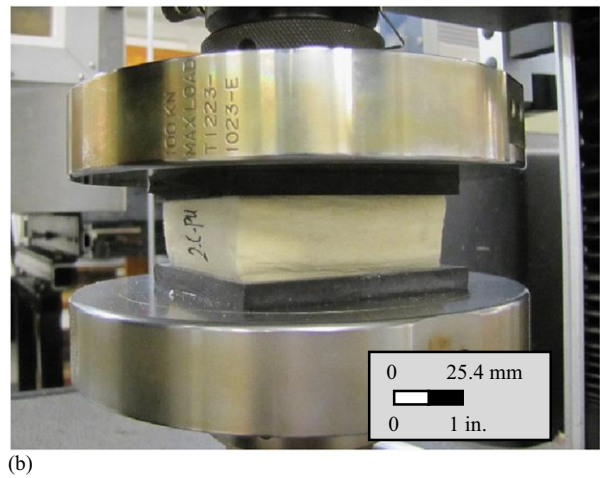
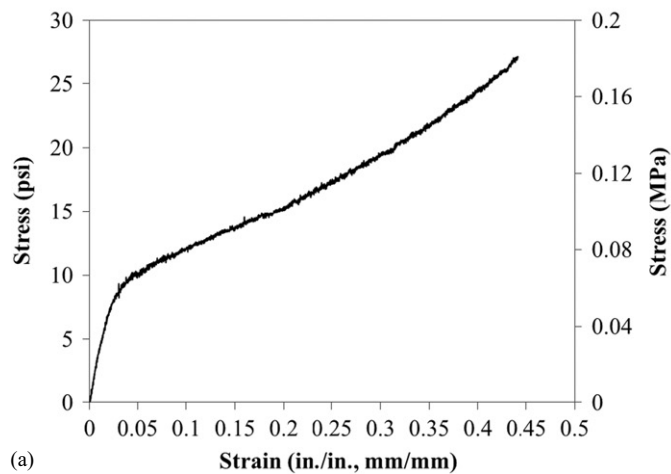


**Fig. 6.** Flatwise compressive test: (a) average compressive stress–strain curves; (b) test setup

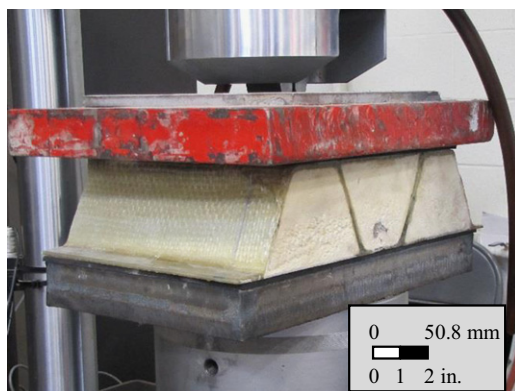


**Fig. 7.** Crushing test setup

the base and spaced 1092.20 mm (43 in.) apart. For the loading beam, two HSS hollow steel sections were welded laterally and gripped to the movable loading head of the MTS-880 machine. Load distribution was accomplished with 50.80 mm (2.0 in.) steel plates that rotated freely around the 25.40 mm (1.0 in.) steel rods. Rubber pads with a shore A hardness of 60 were placed between the specimen and the contact points to avoid stress concentrations.

Axial strains were measured using high precision strain gauges that had a gauge length of 3.18 mm (0.125 in.) and a resistance of 350  $\Omega$ , produced by Micro Measurements Group. Eight strain gauges monitored the strain in the top and bottom facings and throughout the specimen depth. In addition, the displacements at ten locations were monitored by eight direct current variable transformers (DCVTs) and two linear variable differential transformer (LVDT) transducers. The locations of the DCVTs, LVDTs, and strain gauges are shown in Fig. 10.

### Fatigue Test Setup

The fatigue test was conducted on three sandwich panels to assess the service life of the bridge deck under a repeated load. Shenoi et al. (1997) studied the fatigue behavior of FRP composite sandwich beams with a foam core. They concluded that loading configuration, load frequency, and waveform type did not significantly affect the fatigue results. In the current study, three specimens were fatigued at two different load levels. The panel designation included a combination of letters and numbers: FP for fatigued panels; 1, 2, and 3 for the three individual specimens

(written on the left side of the letters); 1, 1.2, 2 indicate the number of cycles in millions (written on the right side of the letters), and 20 and 45 are the peak loads as a percentage of the ultimate load (i.e., 20 represents a peak cyclic load of 20% of the panel ultimate strength). Specimens 1-FP-20-1 and 2-FP-20-2 were subjected to 1 and 2 million loading cycles, respectively, under 20% ultimate load capacity, as suggested in the American Concrete Institute (ACI) 440-2R-08 standard (ACI 2008). Specimen 3-FP-45-1.2 was loaded similarly to the other specimens, but the amplitude of the load was equal to 45% of the ultimate load under 1.2 million cycles. The 2 million cycles' fatigue value was based on the suggestion of AASHTO (2007) for steel bridge components. A 5% threshold of the ultimate load was chosen as the minimum load for all of the specimens to ensure that the specimens remained in place during the fatigue cycling. The loading regime is summarized in Table 4. The specimen was loaded manually up to the minimum load of 3.96 kN (0.89 kip), and then the fatigue cyclic test started with a sinusoidal wave (with frequency of 4.0 Hz) ranging from the minimum load to maximum load of 15.83 kN (3.56 kip) and 35.63 kN (8.01 kip) for the 20 and 45% fatigue loading protocol, respectively.

The fatigue test was conducted on the MTS-880 universal testing machine using the same test setup and fixture as those used in the static flexural test with only minor adjustments. Steel bars with an L-shape were placed at the four corners of the beam fixture to restrain any lateral movements during testing, as shown in Fig. 11. A gap of approximately 12.70 mm (0.5 in.) was allowed between the L-shaped steel bars and the specimen so that the boundary conditions of the test would not be violated.

The DCVTs, LVDTs, and strain gauges were attached in the same manner as in the static flexural test. On completion of the fatigue test, each sandwich panel was statically tested up to failure under a displacement control of 1.27 mm/min (0.05 in./min). Both the residual ultimate strength and the stiffness degradation were compared with the control results.

### Panel Stiffness Calculations

The classical Euler–Bernoulli beam theory provides reasonable results for sandwich beams with a large span-to-depth ratio. However, it underestimates the deflection when the span-to-depth ratio is relatively small because it ignores transverse shear deformations. The FSDT, which is applicable to shear deformable structures, predicts results that are in closer agreement with

experiments (Carlsson and Kardomateas 2011). Accordingly, this theory was adopted in the analysis to evaluate the test results. Besides standard assumptions of the FSDT, the following additional assumptions were adopted in the analysis:

1. A perfect bond exists between different panel components. This assumption is acceptable for design purposes under service loads.

2. Fiber-reinforced polymer material is homogeneous, isotropic, and linearly elastic up to failure.

Both of these assumptions have been confirmed in the current experimental work.

The beam stiffness was determined according to the transformed area method, which converts the nonhomogeneous panel components into an equivalent homogeneous section (ETABS, CSI 2001).

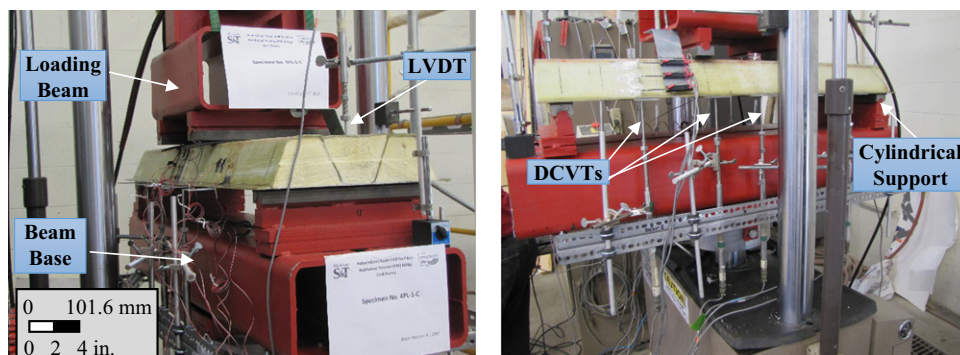


Fig. 8. Four-point bending test setup for the flexure test

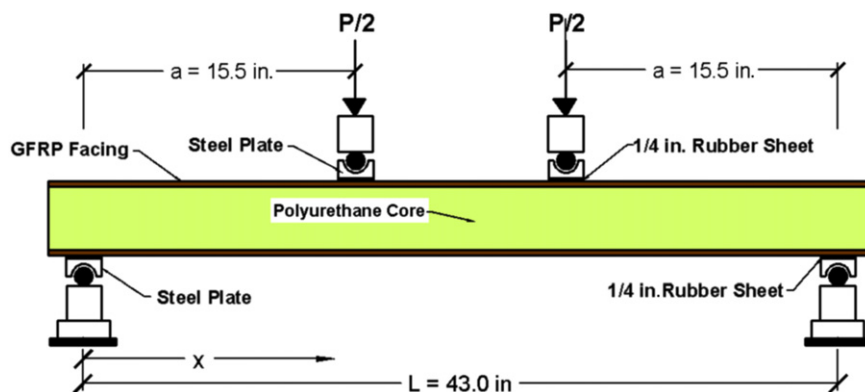


Fig. 9. Schematic of four-point bending test setup; web core perpendicular to the plane of drawing is not shown (all dimensions in inches, 1 in. = 25.4 mm)

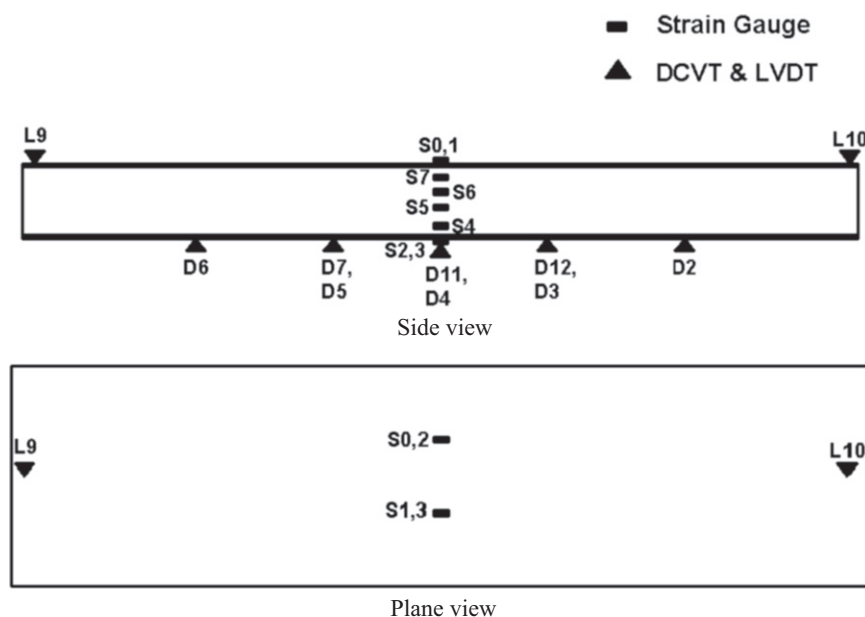
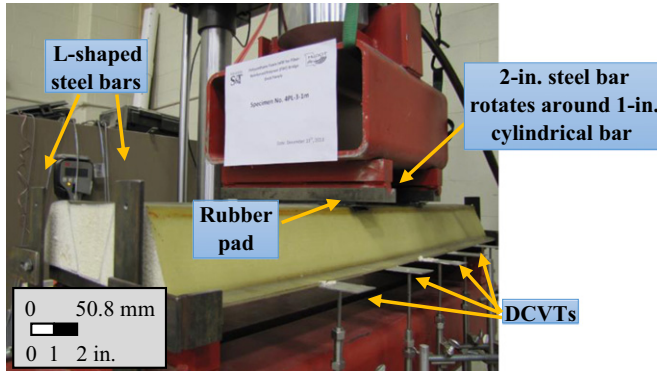


Fig. 10. Schematic of instrumentation locations

**Table 4.** Loading Regime

Load percentage	$P_u = 17.80$ (79.3), kip (kN)
5 (minimum load)	0.89 (3.96)
20 for Specimens 1-FP-20-1 and 2-FP-20-2	3.56 (15.83)
45 for Specimen 3-FP-45-1.2	8.01 (35.63)

**Fig. 11.** Four-point bending test setup for the fatigue test

Because the foam elastic compressive modulus was only approximately 0.02% of the compressive modulus of the GFRP facing and webs, the foam's contribution to the stiffness was ignored in the calculations. The stiffness was calculated by first computing the transformation factor and modular ratio  $n$ , as illustrated in Eq. (1)

$$n_i = \frac{E_i}{E_{sw}} \quad (1)$$

where  $E_{sw}$  = GFRP web's modulus of elasticity; and  $E_i$  =  $i$ th constituent modulus of elasticity. The material properties used in these calculations were based on the coupon tests, as presented in Tables 1–3. The transformed section's moment of inertia,  $I_{tr}$ , was determined according to the elastic neutral axis, as illustrated in Eqs. (2)–(4). Eq. (4) represents the overall effective bending stiffness, which can be obtained by summing the contributions for each part of the construction

$$A_{tr,i} = n_i \times A_i \quad (2)$$

$$\bar{y} = \frac{\sum_{i=1}^n A_{tr,i} \cdot y_i}{\sum_{i=1}^n A_{tr,i}} \quad (3)$$

$$E_e I_{tr} = \sum_{i=1}^n E_i [I_{tr,i} + A_{tr,i} (y_i - \bar{y})^2] \quad (4)$$

where, for component  $i$ ,  $A_i$  = cross-sectional area;  $A_{tr,i}$  = transformed area;  $y_i$  = distance from the center of gravity of the component to the extreme lower fiber;  $E_i$  = modulus of elasticity;  $I_{tr,i}$  = moment of inertia of the transformed section;  $E_e$  and  $I_{tr}$  = effective modulus of elasticity and the effective moment of inertia, respectively, for the entire section; and  $\bar{y}$  = distance from the neutral axis of the transformed cross section to the extreme lower fiber. After determining the location of the neutral axis of the transformed section using Eq. (3), section elements were divided into compression and tension regions so that they corresponded to their material properties. The transformed moment of inertia for each component was then determined, and the overall bending stiffness of the sandwich panel was calculated with Eq. (4).

Once this step was complete, the FSDT could be implemented by using the homogenized bending stiffness calculated from Eq. (4). Both the loading configuration and the panel dimensions

are given in Fig. 10. The expressions for the bending and shear force are presented as follows, respectively:

$$M_{xx} = -E_e I_{tr} \frac{\partial \varphi}{\partial x} \quad (5)$$

$$Q_x = kAG \left( -\varphi + \frac{\partial w}{\partial x} \right) \quad (6)$$

Eqs. (5) and (6) can be integrated, accounting for the boundary conditions corresponding to simple support. Deflection along the panel could then be computed using Eqs. (7) and (8):

$$w(x) = \frac{Px^3}{12E_e I_{tr}} + \frac{Pa^2x}{4E_e I_{tr}} - \frac{PaLx}{4E_e I_{tr}} - \frac{Px}{2kGA} \quad \text{for } 0 \leq x \leq a \quad (7)$$

$$w(x) = \frac{Pa^3}{12E_e I_{tr}} + \frac{Pax^2}{4E_e I_{tr}} - \frac{PaLx}{4E_e I_{tr}} - \frac{Pa}{2kGA} \quad \text{for } a \leq x \leq L - a \quad (8)$$

where  $M_{xx}$  = bending moment along the  $x$ -axis;  $Q_x$  = transverse shear force;  $\varphi$  = angle of rotation of the normal to midsurface of the beam;  $w(x)$  = displacement along the  $x$ -axis;  $P$  = applied load;  $L$  = span length;  $a$  = distance between the support and the loading point (see Fig. 9);  $k$  = shear correction factor (assumed = 5/6); and  $AG$  = effective shear stiffness of the core, which includes the foam and web layer.

The bending stiffness of the tested sandwich panels was also determined by fitting the experimental results to those generated by the FSDT. The polyurethane foam, web, and facings were modeled as isotropic materials. According to the theory of shear deformable beams, the bending stiffness of the sandwich panels was computed accounting for deformations due to bending and transverse shear. The bending stiffness can be determined using the experimental values of deflections at loading point and midspan locations and solving Eqs. (9) and (10) (Carlsson and Kardomateas 2011). A summary of the corresponding results is given in Table 6.

$$\Delta_{\text{midspan}} = \frac{Pa^3}{3EI} - \frac{Pa^2L}{4EI} - \frac{Pa}{2kAG} \quad \text{for } 0 \leq x \leq a \quad (9)$$

$$\Delta_{\text{loading point}} = \frac{Pa^3}{12EI} - \frac{PaL^2}{16EI} - \frac{Pa}{2kAG} \quad \text{for } a \leq x \leq L - a \quad (10)$$

where  $EI$  = bending stiffness of the panel using the experimental values.

## Results and Discussion

### Crushing Behavior

Fig. 12 illustrates the average load–deflection curve for the flatwise crushing tests. The initial nonlinear portion of the curve occurred because of small gaps in the system and can therefore be ignored. The curve exhibited a linear response up to the point at which the foam started to crack at an average load of 77.84 kN (17.5 kip). A noise that was heard during the test revealed that the webs began to buckle at a load of approximately 99.2 kN (22.3 kip) corresponding to an average compressive stress of 0.88 MPa (127 psi). Because the width of the panel varied throughout the cross section, an effective surface area of the panel was difficult to define. Thus, the average compressive stress was calculated by dividing the buckling load by the surface area at the neutral axis. All of the specimens failed in the same manner, as illustrated in Fig. 13. The results, however, exhibited a large

scatter in the ultimate compressive stress, as shown by the high standard deviations and coefficients of variation in Table 5. This high variability occurred because each panel was cut from different larger panels, each of them having slightly different manufacturing defects. These manufacturing defects, although relatively minor, resulted in significant variation across the different specimen samples. It is worth noting that the quality of the panels improved as the specimens size increased. Moreover, improvements in the manufacturing occurred because of the learning curve associated with constructing the specimens in the Missouri S&T Composites Lab. Finally, a composite manufacturer was able to produce full-scale deck panels using the concept presented in this manuscript with consistent characteristics and without significant defects.

### Static Flexural Behavior

Fig. 14 illustrates the load–deflection curves for the two sandwich panels that were subjected to four-point loading tests. The deflection was measured with the DCVTs placed along the two edges at midspan. All specimens were loaded to failure. The behavior of each specimen was nearly linear up to failure; a slight reduction was observed in stiffness prior to failure. The linear response was expected considering the behavior of the individual materials used to manufacture the panels, which are brittle in nature and typically respond in a linear elastic fashion up to failure. Fig. 15 illustrates the

deflection profile for the two specimens. The maximum vertical deflection for Panels 1-CP and 2-CP at midspan measured 26.42 mm (1.04 in.) and 24.89 mm (0.98 in.) at failure loads of 81.22 kN (18.26 kip) and 77.39 kN (17.40 kip), respectively. Table 6 summarizes the results of the static flexural test for each specimen. A popping noise was heard for both panels at the load of approximately 56.94 kN (12.8 kip) and the deflection of 19.05 mm (0.75 in.), as some of the fibers at the top surface of the middle cell [Fig. 16(a)] debonded from the core. This debonding occurred at the section between the loading points and was accompanied by the loud popping noise. At the load of 79.31 kN (17.83 kip), a louder noise was heard, which was associated with local crushing of the facing under one of the loading points, as illustrated in Figs. 16 (b and c). At this point, the test was stopped because the load dropped significantly, reflecting failure of the specimen.

It is worth noting that bridge deck elements have deflection limits that are intend to ensure the element functions properly and does not cause discomfort to individuals using the structure. According to AASHTO and FHWA guidelines, the deflection of bridge deck need to be smaller than 1/800 of the supporting span length. If this limit is applied using the span length of 43 in., the deflection limit state for the investigated FRP panel is 0.054 in., which is significantly smaller than the deflection of the investigated panel at its peak flexural strength, indicating that the design of these panels will likely be controlled by flexural stiffness and serviceability rather than strength. This result was also expected considering the results of testing other types of GFRP bridge decks available in the literature.

The maximum tensile strain recorded at the bottom facing was 0.00907 mm/mm (in./in.) at a load of 79.31 kN (17.83 kip), which represents 53% of the ultimate tensile strain obtained from the

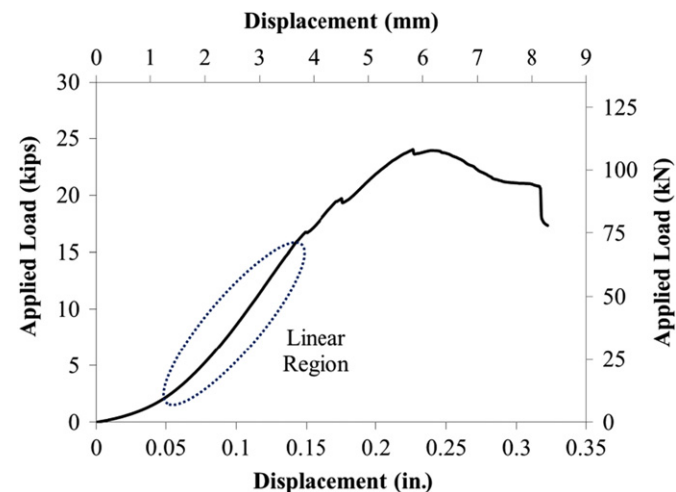


Fig. 12. Average load–displacement curve for crushing test

Table 5. Summary of Crushing Test Results

Specimen no.	Failure load, kN (kip)	Compressive stress, MPa (psi)	Compressive strain, mm/mm, in./in.
1	132.1 (29.7)	1.17 (169.7)	0.054
2	88.9 (20.0)	0.78 (114.3)	0.065
Mean	110.3 (24.8)	0.98 (142.0)	0.059
SD	30.2 (6.8)	0.27 (39.2)	0.0075
COV	27.6	27.6	12.5

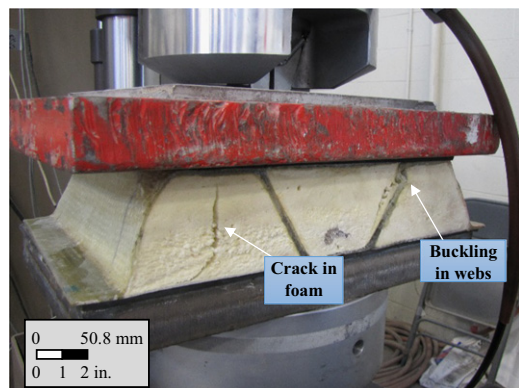


Fig. 13. Failure of specimen subject to crushing test

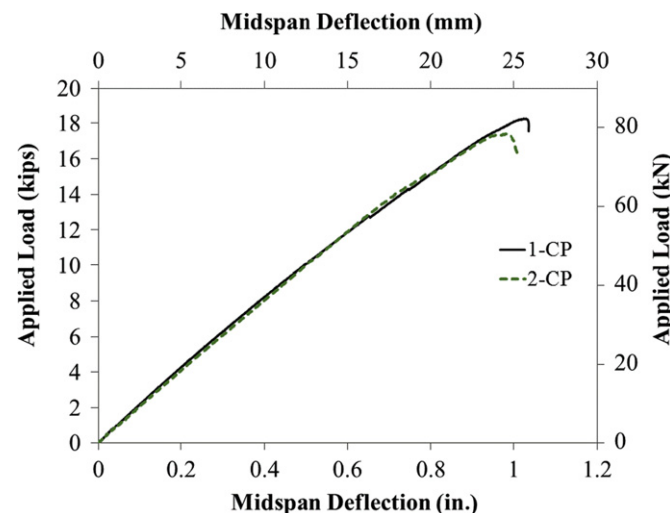
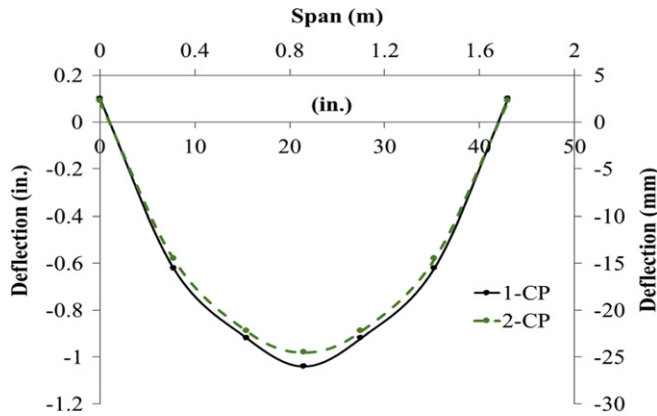


Fig. 14. Load versus midspan deflection for flexure test

tensile coupon tests of the GFRP facing [0.019 mm/mm (in./in.)]. This is consistent with visual inspection, where no cracks were observed at the bottom facing. Rather, failure initiated because of

debonding that started at the top compression surface. As a result, the top face began to wrinkle outward. This phenomenon is also visible in the strain gauge readings at the top face (Fig. 17). These readings exhibited nonlinearity, reversing their direction at approximately  $-0.00365$  mm/mm (in./in.). After the onset of wrinkling, the sandwich panel continued to carry the applied load with a reduced stiffness until failure. The final failure was caused by local crushing of the compressed facing under one of the loading points due to excessive compressive strains.

Four strain gauges (S4, S5, S6, and S7) were glued along the specimen's thickness to monitor the longitudinal strain variation. These measurements validated the assumption that plane sections remained plane during loading. The longitudinal strains were linear up to failure, regardless of their location along the thickness, as shown in Fig. 18. When the strains for different load ranges were plotted, as illustrated in Fig. 19, the neutral axis for the panel section was found to be 63.25 mm (2.49 in.) from the bottom face of the panel. Using the elastic beam theory and transformed section (without considering the foam) resulted in the position of the neutral axis at 60.96 mm (2.4 in.) from the bottom facing, representing 96% of the measured value.



**Fig. 15.** Deflection profile along span length during flexure test

**Table 6.** Summary of Static Flexure Test Results

Specimen no.	$P_u$ , kN (kip)	$\Delta_{\text{midspan}}$ , mm (in.)	$\Delta_{\text{loading point}}$ , mm (in.)	$EI$ , kN.m <sup>2</sup> (kip · in. <sup>2</sup> )	GA, kN (kip)	$\sigma_{\text{skin-bot}}$ , MPa (ksi)	$\tau$ , MPa (ksi)
1-CP	81.2 (18.26)	26.42 (1.04)	23.87 (0.94)	7,310 (25472.7)	$\sim\infty$	105.35 (15.28)	1.28 (0.185)
2-CP	77.4 (17.40)	24.89 (0.98)	22.61 (0.89)	7739.8 (26970.0)	$\sim\infty$	100.39 (14.56)	1.21 (0.175)
Mean	79.3 (17.83)	25.65 (1.01)	23.24 (0.915)	7,525 (26221.4)	$\sim\infty$	102.87 (14.92)	1.24 (0.18)
SD	1.9 (0.43)	0.76 (0.03)	0.64 (0.025)	214.8 (748.65)	—	2.48 (0.36)	0.034 (0.005)
COV	2.41	2.97	2.73	2.86	—	2.4	2.7

Note: COV = coefficient of variation; SD = standard deviation.

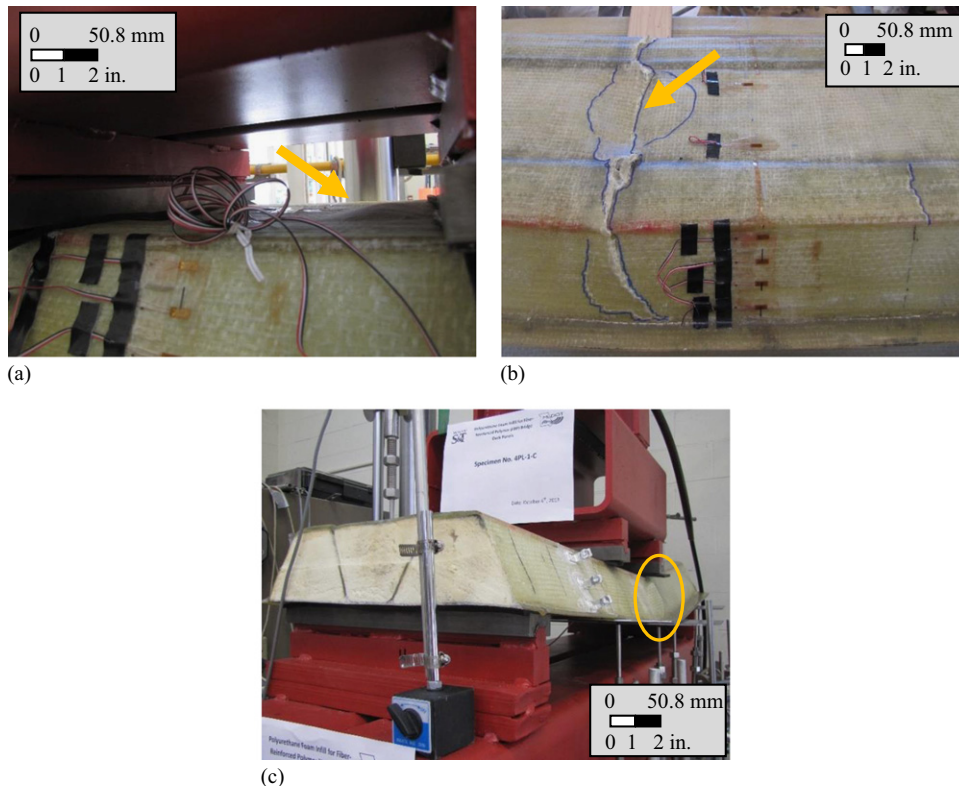


**Fig. 16.** Failure modes: (a) initial failure due to outward compression facing wrinkling; (b) ultimate failure due to compression failure of the facing under loading point; and (c) final failure mode triggered by crushing

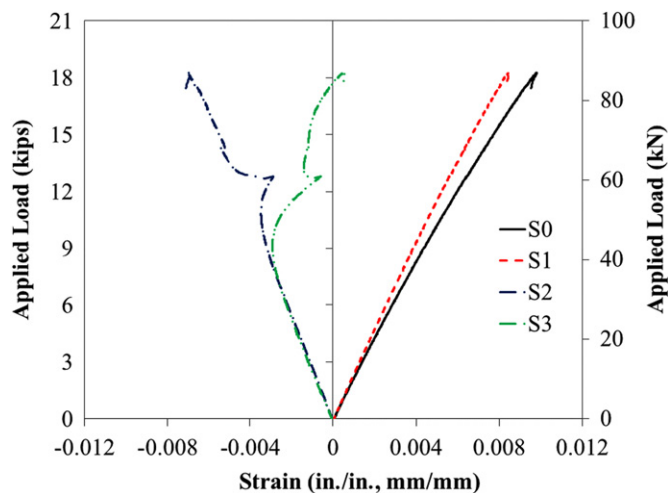


Fig. 17. Load-strain curves for the top and bottom facings

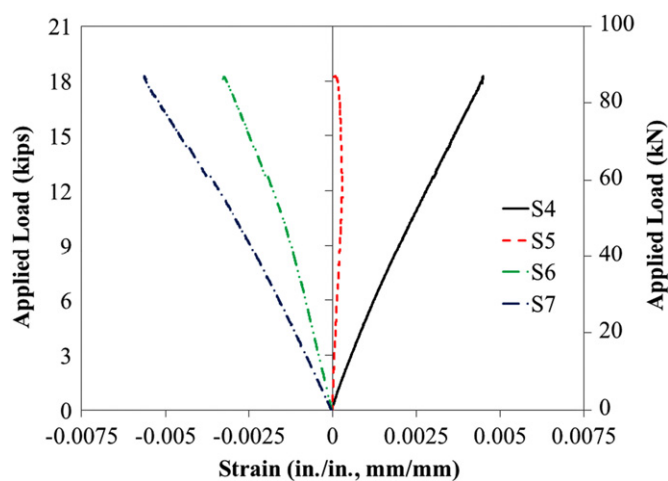


Fig. 18. Load-strain behavior of sandwich panel

### Fatigue Behavior

The residual stresses, stiffness degradation, and failure mode of the tested fatigue specimens were also investigated. After the predetermined number of cycles was reached, each panel was statically tested in the same loading configuration as that used for the control sandwich panels. The stiffness degradation due to fatigue was calculated as the ratio of the stiffness of the fatigued specimen to that of the control specimen that was tested statically.

For all panels, no signs of surface cracks or collapse occurred during the fatigue test. Fig. 7 summarizes the results of the fatigue flexural loading test for each specimen. Fig. 20 illustrates the load versus midspan deflection curves for both fatigued and control specimens. The behavior of the fatigued panels is identical to those tested monotonically (control panels). The maximum deflection for Panels 1-FP-20-1 and 2-FP-20-2 was 31.75 mm (1.25 in.) and 24.13 mm (0.95 in.), respectively, and for Panel 3-FP-45-1.2, the value was 30.48 mm (1.2 in.), whereas the maximum average deflection for the control panels was 25.65 mm (1.01 in.) However, the ultimate load capacities increased by 31.5, 14.6, and 34%, respectively, compared with the control panels. Note that the fatigue test was stopped at 1.2 million cycles for Panel 3-FP-45-1.2 owing to mechanical difficulties with the MTS test machine.

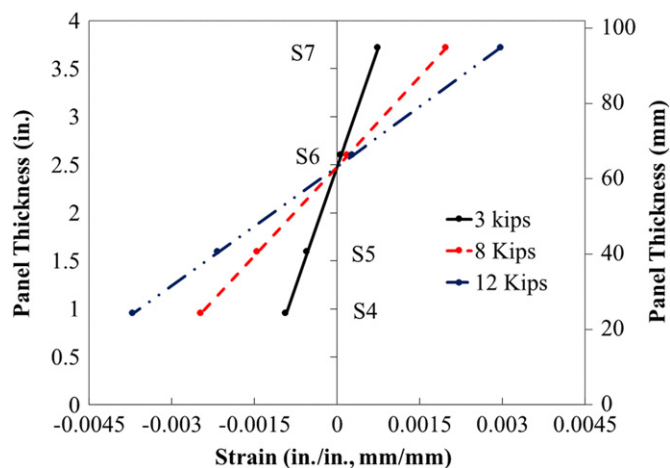


Fig. 19. Strain distribution through the thickness for strain gauges S4, S5, S6, and S7

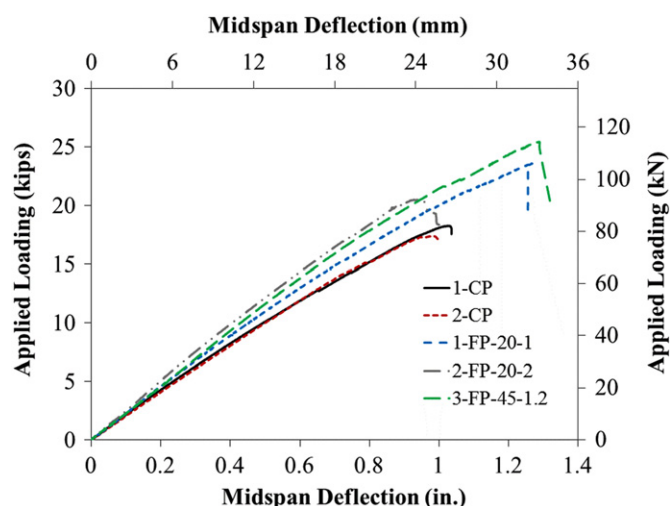
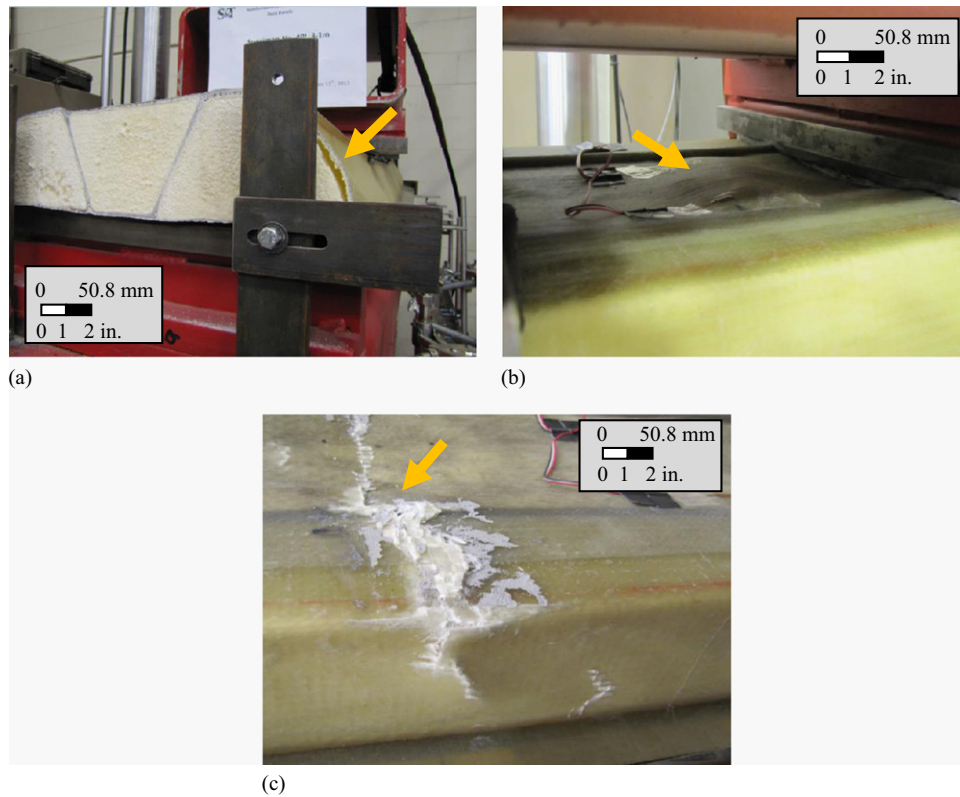


Fig. 20. Load versus midspan deflection for control and fatigued panels

In general, no stiffness reduction was detected in any of the three specimens. Each specimen failed in a manner similar to the control panels. However, a delamination failure occurred prior to the ultimate failure [Fig. 21(a)] between the foam and the GFRP facing at the four corners after the outward facing wrinkled, as illustrated in Figs. 21(b and c). Delamination started at the outer corners of the webs only where shear layers were not provided. This failure mode, which was not observed in statically loaded panels, was introduced only under fatigue loading. Fig. 22 illustrates both the residual bending rigidities and the residual ultimate load for all tested panels. The results indicate that the panels that were conditionally fatigued the most exhibited a higher bending stiffness. The increase in stiffness and strength can be explained by the enhancement of polymer linkages in the FRP material. This enhancement is due to the process where the fatigue loading aligns or reorganizes the polymer linkages so that minor defects in the material are eluded, which has been reported by Rocca and Nanni (2005).

### Comparison of FSDT and Experimental Results

Fig. 23 compares the force-deformation curves calculated using FSDT and those obtained from the experimental results. In



**Fig. 21.** Failure modes: (a) delamination; (b) outward facing wrinkling; and (c) compression failure

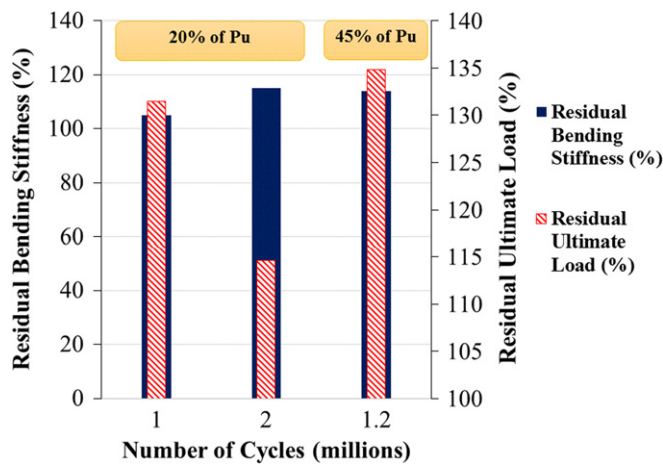


**Fig. 22.** Residual stiffness and strength over fatigue life

general, the FSDT slightly overestimated the bending stiffness and underestimated the expected deflection. The predicted stiffness and deflection using FSDT represents 106.7 and 85% of those measured using the experimental work, respectively. This variation likely occurred for two reasons. First, although the panel section's thickness varied with a coefficient of variation of 7.2%, only one nominal thickness for each component (see Fig. 2) was used in the theoretical calculation. Second, FSDT assumes a perfect bond between the facings, web, and foam. However, debonding at the top facing occurred during the experiment, resulting in stiffness degradation.

The bending stiffness of each investigated panel was computed using Eqs. (9) and (10) of FSDT through the recorded deflections at midspan and at loading points from the experimental work.

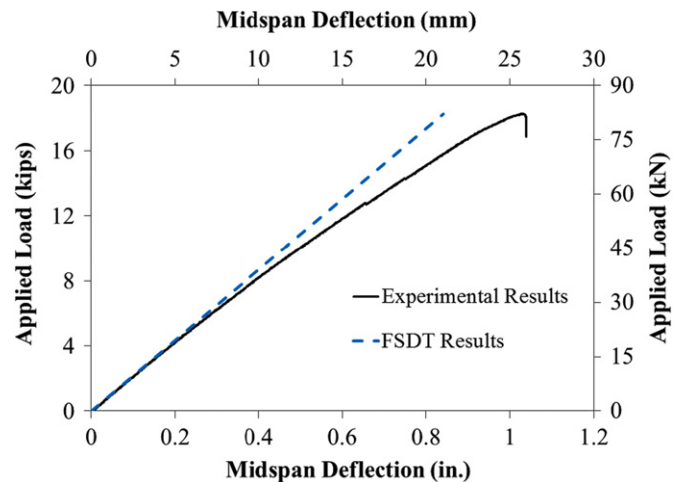


**Fig. 23.** Comparison between experimental results and theoretical predictions by the FSDT theory

Results are presented in Tables 6 and 7. It was found that the shear deformation is minimal. This occurred because the core webs significantly increased the shear stiffness and therefore decreased the shear deformation.

### Conclusions

This study investigated the structural behavior of a new type of sandwich panels with a polyurethane-filled web core. The investigation focused on the new prototype system utilizing a new thermoset polyurethane resin as well as supplemental web shear layers of GFRP. The new resin system that has a longer pot life

**Table 7.** Summary of Fatigue Flexure Test Results

Specimen series	Number of load cycles (millions)	Ultimate load, MPa (ksi)	Midspan deflection, mm (in.)	Flexural stiffness, kN · m <sup>2</sup> (kip · in. <sup>2</sup> )
1-FP-20-1	1	161.3 (23.4)	31.75 (1.25)	7,886.7 (27532.4)
2-FP-20-2	2	140.7 (20.4)	24.13 (0.95)	8,637.8 (30154.6)
3-FP-45-1.2	1.2	165.5 (24.0)	30.48 (1.20)	8,562.7 (29,892.3)

was successfully implemented in the VARTM process to fabricate the panels. The test results demonstrated that the polyurethane resin exhibited superior performance in both static and dynamic tests. The shear layers contributed significantly to enhancing the structural response and shear stiffness; they also delayed delamination of the facings from the core. Excellent bond between different components of the panel was observed. A local outward wrinkling phenomenon, however, was observed between the core and the top facing of the middle cell. This wrinkling could be avoided by increasing the number of plies of the top facing. This prototype system, in general, reduced both the construction time and the initial cost compared with conventional honeycomb sandwich panels. The accuracy of existing analytical models predicting the sandwich panel deflection was also examined. The following conclusions can be drawn:

1. The behavior of the plain-weave facings under tension exhibited a linear elastic response, whereas the web layers where the fibers were oriented at  $\pm 45^\circ$  behaved nonlinearly. Both the facing and web layers behaved almost linearly under compression.
2. The crushing test provided the ultimate bearing capacity, which occurred owing to buckling of the web. The failure load during the four-point loading test was lower than the ultimate bearing capacity. Hence, the buckling in the web core did not occur in the four-point loading test.
3. All panels tested in four-point bending exhibited a linear elastic behavior up to failure. A slight reduction in stiffness due to minor outward skin wrinkling was observed prior to failure. Failure occurred because of local crushing under the applied load.
4. Introducing corrugated webs (shear layers) is an effective way to increase both the core shear stiffness and the global flexural stiffness in the longitudinal direction.
5. In the static flexural test, the maximum strain readings from the bottom gauges of the tested panel indicated that the panel was stressed at 47% of its ultimate capacity as determined from the coupon tests, which is consistent with the outward skin-wrinkling failure mode of the top facing. In other words, the skin-wrinkling failure mode occurs at a lower stress level than the ultimate capacity.
6. The accuracy of the FSDT to predict the deflection of the panels was examined leading to the following conclusions:
  - a. The FSDT overestimated stiffness and underestimated deflection.
  - b. The average difference between the measured deflections and the FSDT results ranged from 6 to 13%.
7. After conditioning the sandwich panels to the predetermined fatigue cycles at the stress levels representing 20 and 45% of their ultimate load, it was observed that no degradation occurred in either bending stiffness or strength. However, delamination failure was observed as an additional failure mode in panels experiencing fatigue loading that was not present in the control panels.
8. The proposed sandwich panel prevented or reduced the facing–core debonding trend observed in conventional sandwich panel construction.

## Acknowledgments

The authors would like to acknowledge the support provided by the Missouri Department of Transportation (MoDOT) and the National University Transportation Center (NUTC) at Missouri University of Science and Technology.

## References

- AASHTO. (2007). *AASHTO LRFD bridge design specifications, SI Units*, 4th Ed., Washington, DC.
- Abdelkarim, O., and ElGawady, M. A. (2014). "Analysis and finite element modeling of FRP-concrete-steel double-skin tubular columns." *J. Bridge Eng.*, 10.1061/(ASCE)BE.1943-5592.0000700, B4014005.
- ACI. (2008). "Guide for the design and construction of externally bonded FRP systems for strengthening concrete structures." *440.2R – 08*, Farmington Hills, MI.
- ASTM. (2008a). "ASTM standard test method for tensile properties of polymer matrix composite materials." *ASTM D3039/D3039M-08*, West Conshohocken, PA.
- ASTM. (2008b). "ASTM standard test method for compressive properties of polymer matrix composite materials with unsupported gage section by shear loading." *D3410/D3410M-03*, West Conshohocken, PA.
- ASTM. (2011a). "ASTM standard test method for flatwise compressive properties of sandwich cores." *C365/C365M-11a*, West Conshohocken, PA.
- ASTM. (2011b). "ASTM standard test method for flexural properties of sandwich constructions." *C393/C393M-11e1*, West Conshohocken, PA.
- Camata, G., and Shing, P. B. (2010). "Static and fatigue load performance of a GFRP bridge deck." *Composites Part B*, 41(4), 299–307.
- Carlsson, L. A., and Kardomateas, G. A. (2011). *Structural and failure mechanics of sandwich composites*, Springer, New York.
- Connolly, M., King, J., Shidaker, T., and Duncan, A. (2006). *Processing and characterization of pultruded polyurethane composites*, Huntsman, Polyurethanes, Auburn Hills, MI.
- Dawood, H., and ElGawady, M. A. (2013). "Performance-based seismic design of unbonded precast post-tensioned concrete filled GFRP tube piers." *Composites Part B*, 44(1), 357–367.
- ElGawady, M. A., Booker, A. J., and Dawood, H. (2010). "Seismic behavior of posttensioned concrete-filled fiber tubes." *J. Compos. Const.*, 10.1061/(ASCE)CC.1943-5614.0000107, 616–628.
- ElGawady, M. A., and Dawood, H. M. (2012). "Analysis of segmental piers consisted of concrete filled FRP tubes." *Eng. Struct.*, 38, 142–152.
- ElGawady, M. A., and Sha'lan, A. (2011). "Seismic behavior of self-centering precast segmental bridge bents." *J. Bridge Eng.*, 10.1061/(ASCE)BE.1943-5592.0000174, 328–339.
- ETABS, CSI. (2001). *Technical note transformed section moment of inertia. Composite beam design AISC-ASD89*, Computers and Structures, Berkeley, CA.
- Hassan, T., Reis, E. M., and Rizkalla, S. H. (2003). "Innovative 3-D FRP sandwich panels for bridge decks." *Proc., 5th Alexandria Int. Conf. on Structural and Geotechnical Engineering*, Alexandria, Egypt, 20–22.
- Ji, H. S., Song, W., and Ma, Z. J. (2010). "Design, test and field application of a GFRP corrugated-core sandwich bridge." *Eng. Struct.*, 32(9), 2814–2824.

- Kirk, R. S., and Mallett, W. J. (2013). "Highway bridge conditions: Issues for Congress." *Rep. No. R43103*, Congressional Research Service, Washington, DC.
- Murton, M. C. (1999). "Commercialization of FRP bridge decks: Lessons and challenges for Ohio's project 100." *Proc. Int. SAMPE Symp. Exhibition*, 46(1), 943–951.
- Potluri, P., Kusak, E., and Reddy, T. Y. (2003). "Novel stitch-bonded sandwich composite structures." *Compos. Struct.*, 59(2), 251–259.
- Rocca, S. V., and Nanni, A. (2005). "Mechanical characterization of sandwich structure comprised of glass fiber reinforced core: Part 1." *Composites in Construction: 3rd Int. Conf.*, Lyon, France, 11–13.
- Shenoi, R. A., Allen, H. G., and Clark, S. D. (1997). "Cyclic creep and creep-fatigue interaction in sandwich beams." *J. Strain Anal.*, 32(1), 1–18.
- Zi, G., Kim, B. M., Hwang, Y. K., and Lee, Y. H. (2008). "An experimental study on static behavior of a GFRP bridge deck filled with a polyurethane foam." *Compos. Struct.*, 82(2), 257–268.